2D Materials

OPEN ACCESS

RECEIVED
22 July 2025

REVISED
23 October 2025

ACCEPTED FOR PUBLICATION
15 December 2025

PUBLISHED
20 February 2026

Original content from this work may be used under the terms of the Creative Commons Attribution 4.0 licence.

Any further distribution of this work must maintain attribution to the author(s) and the title of the work, journal citation and DOI.

PAPER

A large interlaboratory electron diffraction study of monolayer graphene

Evan Tillotson[1,2], William Thornley[1,2], William Talbott[1,2], Alexander S Eggeman[1], Daria Kriuchkova[1], Sam Sullivan-Allsop[1,2], Matt Smith[1], Xuzhao Liu[1], Ashley Slattery[4], Pei Lay Yap[4], Dusan Losic[4], Zhun Xu[5], Huan Wang[5], Jim Ciston[6], Alexander Rakowski[7], Stephanie M Ribet[7], Benjamin H Savitzky[7], Manfred E Schuster[8], Christopher S Allen[9,25], Danielle Douglas-Henry[10], Valeria Nicolosi[10], Andrew Herzing[11], Jacques O'Connell[12], Ezra J Olivier[12], Jan Neethling[12], Yi-Chao Zou[13], Ercin Duran[14], Rongsheng Cai[15], Duc-The Ngo[1], Roman Gorbachev[2,16], Jonas Haas[17,18], Michael Schlegel[17,18], Jannik Meyer[17,18], Alba Centeno[19], Amaia Pesquera[19], Amaia Zurutuza[19], Sungsu Kang[20], Jungwon Park[20], Ivan Erofeev[21], Utkur Mirsaidov[21], Colin Ophus[22], Christian Rentenberger[23], Thomas Waitz[23], Jani Kotakoski[23], Abhijit Roy[24,26], Raul Arenal[24,26,27], Andrew J Pollard[3,*] and Sarah J Haigh[1,2,*]

[1] Department of Materials, University of Manchester, Manchester M13 9PL, United Kingdom
[2] National Graphene Institute, University of Manchester, Manchester M13 9PL, United Kingdom
[3] National Physical Laboratory, Hampton Rd, Teddington TW11 0LW, United Kingdom
[4] School of Chemical Engineering and Adelaide Microscopy, The University of Adelaide, Adelaide, SA, 5005, Australia
[5] College of Chemistry and Molecular Engineering, Peking University, Haidian District, Beijing 100871, People's Republic of China
[6] Molecular Foundry, Lawrence Berkeley National Laboratory, One Cyclotron Road Building 67, Berkeley, CA 94720, United States of America
[7] National Center for Electron Microscopy Facility, Molecular Foundry, Lawrence Berkeley National Laboratory, Berkeley, CA 94720, United States of America
[8] Johnson Matthey Technology Centre, Blounts Court, Sonning Common RG4 9NH, United Kingdom
[9] Electron Physical Science Imaging Centre (ePSIC), Didcot, Oxfordshire, OX11 0DE, United Kingdom
[10] The Centre for Research on Adaptive Nanostructures and Nanodevices, Trinity College Dublin, 43 Pearse St, Dublin 2, D02 W085, Ireland
[11] National Institute of Science and Technology, 100 Bureau Drive, Gaithersburg, MD 20899, United States of America
[12] Centre for HRTEM, Department of Physics, Nelson Mandela University, Gqeberha 6001, South Africa
[13] School of Materials Science and Engineering, Sun Yat-sen University, Guangzhou 510275, People's Republic of China
[14] Department of Metallurgical and Materials Engineering, Istanbul Technical University, Istanbul 34469, Türkiye
[15] State Key Laboratory of Solid Lubrication, Lanzhou Institute of Chemical Physics, Chinese Academy of Sciences, Tianshui Middle Road, Lanzhou, Gansu 730000, People's Republic of China
[16] Department of Physics and Astronomy, University of Manchester, Manchester M13 9PL, United Kingdom
[17] Institute of Applied Physics, University of Tuebingen, Auf der Morgenstelle 10, Tübingen 72076, Germany
[18] NMI Natural and Medical Sciences Institute at the University of Tuebingen, Markwiesenstrasse 55, Reutlingen 72770, Germany
[19] Graphenea, Graphenea Headquarters, Paseo Mikeletegi 83, 20009 San Sebastián, Spain
[20] Department of Chemical and Biological Engineering, Institute of Chemical Processes, Seoul National University, Seoul 08826, Republic of Korea
[21] Department of Physics, National University of Singapore (NUS), 14 Science Drive 4, Singapore 117557, Singapore
[22] Department of Materials Science & Engineering, Stanford University, 496 Lomita Mall, Stanford, CA 94305, United States of America
[23] Faculty of Physics, University of Vienna, Boltzmanngasse 5, Vienna 1090, Austria
[24] Instituto de Nanociencia y Materiales de Aragon (INMA), CSIC-University of Zaragoza, Calle Mariano Esquillor, 50018 Zaragoza, Spain
[25] Department of Materials, University of Oxford, Oxford OX1 3PH, United Kingdom
[26] Laboratorio de Microscopias Avanzadas (LMA), University of Zaragoza, Calle Mariano Esquillor, 50018 Zaragoza, Spain
[27] Fundacion ARAID, 50018 Zaragoza, Spain
[*] Authors to whom any correspondence should be addressed.

E-mail: andrew.pollard@npl.co.uk and sarah.haigh@manchester.ac.uk

Keywords: graphene, electron diffraction, 2D materials, transmission electron microscopy, monolayer

Supplementary material for this article is available online

© 2026 The Author(s). Published by IOP Publishing Ltd

Abstract

Standardisation of data collection and analysis is essential to enable commercialisation of 2D materials in a wide range of technologies. Selected area electron diffraction (SAED) in the transmission electron microscope (TEM) is one of the key methods for distinguishing monolayer from bilayer and few-layer graphene by comparing the 1st and 2nd order diffraction spot intensities. Yet there are many factors that can affect the reliability of data collection and interpretation, causing the measurement of monolayer samples to deviate from the literature boundary condition of $I_{\{\bar{2}110\}}/I_{\{1\bar{1}00\}} < 1$ for monolayer graphene (1LG). Here we present the results of a large interlaboratory SAED comparison study, where 15 international laboratories measured and analysed nominally identical samples of chemical vapour deposited graphene. Large variations were observed in the measured ratios of diffraction spot intensities, with the largest variance associated with poor quality SAED data resulting from inadequate specimen handling and storage. To inform the reliable determination of monolayer thickness from SAED patterns we provide a description of best practice for specimen handling, TEM operation, data collection and analysis. This work was undertaken within VAMAS Technical Working Area 41: Graphene and related 2D materials—Project 9, the results of which have been directly incorporated into ISO/TS 21356–2 for the characterisation of graphene sheets. We find that when this methodology is followed, 1LG can be distinguished from bilayer or thicker material with high confidence where analysis of a single SAED pattern gives $I_{\{\bar{2}110\}}/I_{\{1\bar{1}00\}} < 1.2$, even in the absence of precise specimen tilting.

1. Introduction

Graphene and other 2D materials have huge commercial potential in broad applications such as gas sensors [1], energy storage [2], filtration membranes and flexible electronics [3, 4]. Yet widespread usage is often held back by the challenges of reliable, standardised characterisation of these materials to enable mass production. One common characterisation challenge is to distinguish monolayer graphene (1LG) from bilayer graphene (2LG), few-layer graphene (FLG) or graphite, since these have marked differences in their mechanical [5] and electronic [6, 7] properties. Raman spectroscopy can probe differences in the quality and thickness of graphene through analysis of the, D-, G- and 2D-peaks [8]. Yet it is typically limited to a lateral spatial resolution of >300 nm [9] so cannot unambiguously determine nanoscale regions of different thickness, which are often present in exfoliated materials as well as graphene sheets produced through chemical vapour deposition (CVD) [10, 11]. Atomic force microscopy (AFM) is capable of sub-nm spatial and height resolution [12], but it is time consuming, and the technique struggles to unambiguously determine monolayer thickness due to the potential for trapped species beneath the sample and the substrate as well as probe artifacts [13].

Transmission electron microscopy (TEM) has the disadvantage that it requires a suspended sample, yet the technique provides unrivalled atomic scale local imaging of structure and chemistry. For example, TEM and scanning TEM (STEM) imaging has been applied to probe edge structures [14], Stone–Wales defects [15, 16], and substitutional impurity atoms [17] in FLG sheets. Furthermore, electron energy loss spectroscopy [18, 19] in the TEM/STEM provides access to local changes in graphene's bonding [20] and can reveal isotopic doping with ^{13}C [21]. However, atomic resolution imaging of 1LG and detailed TEM/STEM spectroscopic analysis both require advanced TEM/STEM instruments that are not widely available, particularly in commercial testing laboratories. Selected area electron diffraction (SAED) in the TEM provides information on local crystal structure at a lower lateral spatial resolution, typically limited to ∼100 nm [22]. Yet, SAED has the advantage that it can survey much larger measurement areas than are investigated with atomic TEM/STEM imaging. It is also routinely accessible on all TEM instruments, less sensitive to precise electron lens alignments and requires less operator training. Seminal work by Meyer *et al* [23, 24] has shown that SAED data collected as a function of specimen tilt along specific crystallographic zone axes allow unambiguous separation of monolayer from 2LG based on differences in the diffraction spot intensities. When tilted along specific crystallographic axes, 1LG shows consistent diffraction spot intensities due to its uniform atomic layer. In contrast, the AB stacking of Bernal-stacked 2LG produces modulated intensities caused by interlayer interactions and stacking effects that alter electron-wave interference. However, collection of SAED patterns while tilting is both experimentally challenging and time consuming, especially for laterally small graphene sheets. Consequently, it has become common practice to determine monolayer from bilayer and thicker graphene using just a single SAED pattern of graphene, obtained with the electron beam close to the [0001] zone axis (perpendicular to the basal plane). Despite significant

progress in the ability to characterise grain boundary configurations in 1LG [25] and strain in twisted bilayers [26] using electron diffraction [27] the confidence of SAED analysis of graphene thickness has not been assessed.

To perform this analysis, the graphene sample must be suspended using a holey support grid and loaded into the vacuum of the TEM. Typically, a single intensity line profile is taken from the hexagonally symmetric SAED pattern to assess the ratio of the intensities of the second order, $I_{\{\bar{2}110\}}$, to first order, $I_{\{1\bar{1}00\}}$, diffraction spots [28]. This approach is appealing in its simplicity and ease of use, but the accuracy is uncertain due to the many experimental factors that can affect SAED spot intensities including specimen tilt, topography, defects, surface contamination, instrumental set-up, acquisition and analysis parameters [24].

Literature agrees that where the $I_{\{\bar{2}110\}}/I_{\{1\bar{1}00\}}$ diffraction ratio is found to be less than or equal to 1 the region being imaged is assigned to 1LG, while a $I_{\{\bar{2}110\}}/I_{\{1\bar{1}00\}}$ value greater than 1 indicates bilayer or thicker graphene [29–36]. This definition predates work by Meyer *et al* [23, 24] and other early studies on the structure of graphene, with the earliest reference related to hexagonal SAED patterns from 'carbon nanofilms' [31]. Despite consistency in setting $I_{\{\bar{2}110\}}/I_{\{1\bar{1}00\}} = 1$ as the boundary condition, there are significant variations in the measured values for monolayer and bilayer reported in the literature. For example, Su *et al* find 1LG to be when $I_{\{\bar{2}110\}}/I_{\{1\bar{1}00\}}$ is 0.71 and a value of 2.5 to be 2LG [29]. Hernandez *et al* report $I_{\{\bar{2}110\}}/I_{\{1\bar{1}00\}}$ is 0.66 for monolayer and 2.85 for multilayer [30]. Kumar *et al* find $I_{\{\bar{2}110\}}/I_{\{1\bar{1}00\}}$ of 0.72 for 1LG [33] and Wang *et al* find $I_{\{\bar{2}110\}}/I_{\{1\bar{1}00\}}$ values of 2 as bilayer [32]. Recently, Zhang *et al* report line profiles measuring $I_{\{\bar{2}110\}}/I_{\{1\bar{1}00\}}$ of 0.55 for graphene monolayers [36].

2LG with the thermodynamically unfavourable AA stacking will exhibit $I_{\{\bar{2}110\}}/I_{\{1\bar{1}00\}}$ ratios similar to monolayer [37]. However, given the rarity of this structure its presence can generally be ignored, as it is in the analysis presented here. Lu *et al* also report that separate graphene monolayers stacked together with an arbitrary rotation angle, known as 'twisted' bilayers, show $I_{\{\bar{2}110\}}/I_{\{1\bar{1}00\}}$ 0.5–0.75 [34], similar to single layer graphene [29, 30] while values of 2.0–2.6 are measured for Bernal stacked bilayer materials [34]. Other work on twisted graphene bilayers by Sun *et al* show $I_{\{\bar{2}110\}}/I_{\{1\bar{1}00\}}$ ratios around $\sim$0.62 [38]. Similar analysis has also been applied to graphene oxide materials, with Wilson *et al* illustrating values of $I_{\{\bar{2}110\}}/I_{\{1\bar{1}00\}}$ $\sim$0.71 in their data [39] and Ren *et al* showing line profiles measuring $I_{\{\bar{2}110\}}/I_{\{1\bar{1}00\}}$ to be 0.55 [40].

Simulated monolayer and bilayer SAED data also yields a range of values for the $I_{\{\bar{2}110\}}/I_{\{1\bar{1}00\}}$ ratios [23, 24]. Such calculations depend not only on the atomic scattering function but also on thermal vibrations, included in simulations through the incorporation of the Debye–Waller factor. Without a Debye–Waller factor the $I_{\{\bar{2}110\}}/I_{\{1\bar{1}00\}}$ ratio for 1LG is unity. Yet thermal vibrations damp higher frequencies to a larger extent, resulting in $I_{\{\bar{2}110\}}/I_{\{1\bar{1}00\}}$ values of less than one. The $I_{\{\bar{2}110\}}/I_{\{1\bar{1}00\}}$ ratios in simulations for 2LG and FLG samples also depend on the choice of Debye–Waller factor as well as the acceleration voltage, as this changes the scattering angles. Precise calculation of the correct Debye–Waller factor for graphene at room temperature requires a number of approximations [41], enabling the Debye–Waller factor to be used as a flexible parameter to enable a close match of the $I_{\{\bar{2}110\}}/I_{\{1\bar{1}00\}}$ values in simulations with those obtained experimentally. We recognise that the presence of point lattice defects can also have the effect of a 'static' Debye–Waller factor as is seen in graphene oxide materials where the high defect density is found to reduce the $I_{\{\bar{2}110\}}/I_{\{1\bar{1}00\}}$ peak ratio [27, 42]. This explains why graphene oxide and other very disordered graphitic samples have a peak ratio that strongly differs from those of clean and highly crystalline graphene samples [43]. Thus, it is challenging to deconvolve the effect of thermal vibrations from the presence of point defects from SAED alone and corroboration with atomic resolution imaging or spectroscopic techniques (e.g. Raman) is required to assess defect density [44].

Building on our previous 'Good Practice Guide 145: Characterisation of the Structure of Graphene' [45], here we consider the accuracy and precision for determining the presence of 1LG with SAED through a large interlaboratory TEM study. This study was run under the auspices of the Versailles Project on Advanced Materials and Standards (VAMAS) through Technical Working Area 41 'Graphene and Related 2D Materials' as Project 9. VAMAS was formed in 1982 to promote the adoption of advanced materials through international collaboration on measurement best practice, allowing the development of accurate and precise international measurement standards. In what we believe to be the largest TEM standardisation interlaboratory study performed to date, 15 international laboratories measured and analysed nominally identical samples of commercially-produced CVD-grown graphene prepared on Quantifoil TEM grids (Graphenea, San Sebastián, Spain) as shown in figure 1(a) (see SI section 1 for details of CVD sample preparation). The coverage of 1LG for these samples was determined to be 97%, assessed by the contrast in optical microscopy images of the as-grown CVD graphene across a silicon/silicon oxide substrate as well as complementary Raman spectroscopy and AFM measurements (see SI figures S1–S4). The bilayer regions observed by optical imaging could be either Bernal- or turbostratically stacked. Here we

discuss the SAED results from the different laboratories, potential sources of uncertainty and how to minimise these. The results have been used to develop the TEM/SAED protocol for the international measurement standard 'structural characterisation of graphene, Part 2: Graphene sheets on a substrate', International Organization for Standardization (ISO) Technical Specification 21356–2, within ISO Technical Committee 229—Nanotechnologies.

2. Internal protocol testing (Phase 1)

In Phase 1 of this study three participants at the University of Manchester, hereafter termed Participant A, B and C, were each provided with different CVD-grown graphene samples on Quantifoil TEM grids as shown in figures 1(a)–(d) and asked to follow the methodology described in a draft standard protocol. Full sample synthesis methods are provided in SI section 1 and the full text of the protocol, including marked-up details of how it was refined during this study, are given in SI section 3. The draft measurement protocol required each participant to bake the graphene TEM grid for >8 h at a pressure $<1 \times 10^{-5}$ mbar to reduce mobile hydrocarbon surface contamination. Then, after checking for obvious defects to the TEM grid using optical microscopy, the participant was told to acquire 10–40 SAED and TEM image pairs, and to record their instrument parameters in a spreadsheet (SI section 3). The participants were not told what to expect in terms of the homogeneity or number of layers of graphene. Tilting to the zone axis was not required due to the high conformity of the CVD graphene with the supporting grid. We also performed precession electron diffraction (PED) studies as these can mitigate the potential impact of local tilt because many tilt angles are summed (SI figure S5). However, PED was not found to significantly alter the diffraction intensity measurements and is more experimentally demanding so is not considered further (see SI figure S5).

The protocol also provided guidance on the analysis of the expected characteristic graphene SAED patterns when assessing if one or more layers of graphene were present. Figures 1(e) and (f) show examples of SAED patterns for monolayer and 2LG single crystals, respectively, each with the characteristic sixfold symmetry expected for viewing perpendicular to the basal plane. Typically published literature only includes the 2D SAED pattern with the $I_{\{\bar{2}110\}}/I_{\{1\bar{1}00\}}$ ratio measured from a single intensity line profile, with this line profile acquired to include two of the six diffraction peaks closest to the central, unscattered beam ('first-order', $\{1\bar{1}00\}$ spots) and two of the next closest six diffraction peaks, 'second-order', $\{\bar{2}110\}$ spots. However, as illustrated in figures 1(e) and (f) there are six possible locations for these intensity line scans on the SAED pattern, and these do not produce identical measurements for $I_{\{\bar{2}110\}}/I_{\{1\bar{1}00\}}$. Factors such as sample tilt, surface contamination, TEM calibrations and alignment errors, the position of the beam stop, and the modulation transfer functions of the TEM camera can all affect the intensity of the diffraction peaks, hence introducing variability in the measured $I_{\{\bar{2}110\}}/I_{\{1\bar{1}00\}}$. To attempt to reduce these effects for a single SAED pattern, the analysis protocol requires participants to measure all 6 equivalent line profiles, as shown in figures 1(e) and (f). The participants were required to record both first-order and second-order diffraction intensities for each profile, then calculate the 'mean ratio of second: first order spots' in each SAED pattern, and also to record 'the standard deviation error' in a spreadsheet. Where the beam stop obscures one of the diffraction peaks, the participant is instructed to use just the remaining peaks when calculating the mean and standard deviation.

Initial analysis of data received from Participants A, B and C in Phase 1 (SI figure S6) revealed an inconsistency in the method used by different participants to calculate both the mean diffraction ratios and the standard deviation for each diffraction pattern. Participants A and B calculated the mean of the second and first order diffraction peaks for each SAED pattern and took the ratio of these two, which we define as m_{pi} for a participant, p and a SAED pattern, i. The standard deviation for each pattern was calculated as the propagated uncertainty on the average standard deviation of all first order peak heights and of all second order peak heights, which we define as s_{pi}. Participant C used an alternative approach and calculated the mean ratio for each of the six line scans, then reported the mean and standard deviation of these means for each pattern. Where there are individual spots missing from the diffraction pattern, these two methods will result in different values for $I_{\{\bar{2}110\}}/I_{\{1\bar{1}00\}}$. The standard deviations will also be vastly different as shown in SI figure S7, with the approach used by Participant C generally giving smaller standard deviation errors as the mean ratio for each line scan already contains averaging, therefore not providing an accurate understanding of the associated uncertainty. To compare the data sets in Phase 1, we have therefore reprocessed the data of Participant C to be consistent with A and B and compare the values of the intensity ratios, m_{pi}, and the standard deviations, s_{pi}, as shown in figure 2(a).

The common assumption of the intensity ratio of diffraction spots, $I_{\{\bar{2}110\}}/I_{\{1\bar{1}00\}}$, measuring less than 1 for 1LG, implies that all of the areas analysed by Participant C are more than one layer thick (as shown in figure 2(a)). This contradicts larger spatial resolution optical imaging and previous Raman analyses (SI figures S1–S3) for these samples. However, the

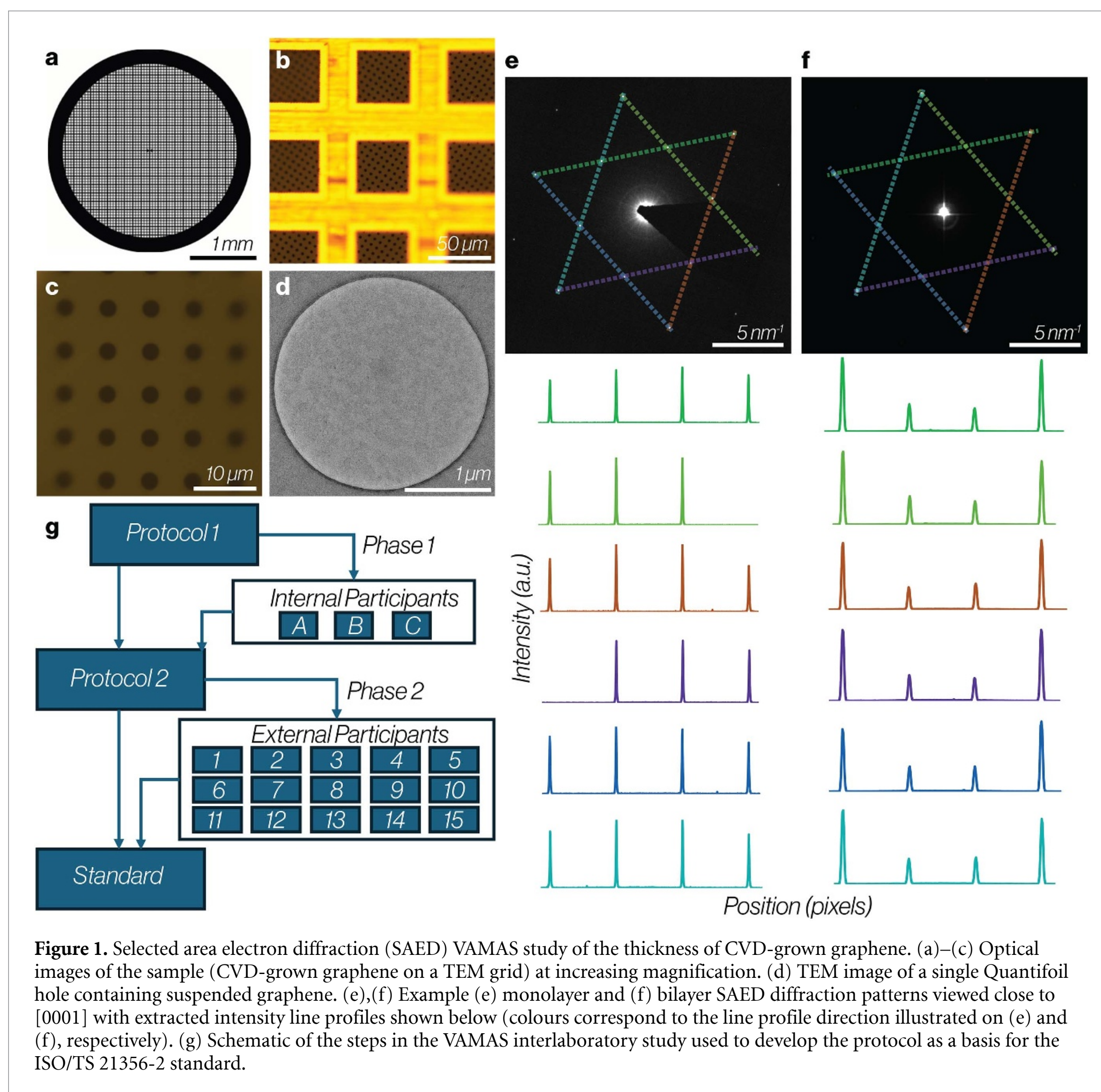

Figure 1. Selected area electron diffraction (SAED) VAMAS study of the thickness of CVD-grown graphene. (a)–(c) Optical images of the sample (CVD-grown graphene on a TEM grid) at increasing magnification. (d) TEM image of a single Quantifoil hole containing suspended graphene. (e),(f) Example (e) monolayer and (f) bilayer SAED diffraction patterns viewed close to [0001] with extracted intensity line profiles shown below (colours correspond to the line profile direction illustrated on (e) and (f), respectively). (g) Schematic of the steps in the VAMAS interlaboratory study used to develop the protocol as a basis for the ISO/TS 21356-2 standard.

standard deviation errors for the intensity ratios are relatively large for all participants, with several reaching 100% of the ratio value itself. To quantify the relative contribution of the many potential sources of uncertainty that could lead to a large variance, we now consider manual analysis of SAED diffraction peaks applied to electron diffraction simulations (see SI Section 4 for details of these multislice simulations [46] implemented on a GPU [47]). Manual analysis of perfect 1LG simulations (without including phonon vibrations) gave the expected value of $I_{\{\bar{2}110\}}/I_{\{1\bar{1}00\}} = 1$ with a standard deviation (s_{pi}) of 0.003 (SI figure S8). Adding a single frozen phonon deviation into the simulation (displacements were described by a Gaussian distribution with a standard deviation of 0.05 Å) reduced the mean intensity ratios to 0.8 with a larger measured s_{pi} of 0.2. More frozen phonon layers would be expected to reduce this uncertainty by increasing the averaging, so this is considered a worst-case scenario, yet it is notable that a $I_{\{\bar{2}110\}}/I_{\{1\bar{1}00\}}$ value greater than 1 is within the uncertainty for 1LG when thermal vibrations are included in the simulations. Nonetheless, the typical uncertainties in the Phase 1 data are much larger than found by similar treatment of simulated data, even with the extreme addition of only a single phonon vibration.

One potential cause of this increased uncertainty is imperfect alignment of the TEM, particularly diffraction astigmatism or poor diffraction focus, which can cause streaking of the diffraction data and change the peak intensities measured in an intensity line profile. Analysis of Participant A's data showed that the Fourier transforms of TEM images were asymmetric (figure 2(c)) and diffraction patterns showed asymmetric streaking of all diffraction spots (figure 2(d)), both suggestive of TEM alignment errors. However, Participants B and C had no obvious symptoms of microscope misalignments yet still had larger uncertainties than the simulations. Another potential cause of increased measurement uncertainty is damage to the graphene sheet. This causes buckling and local variations in sample orientation [23], and can also induce strain in the graphene lattice, visible

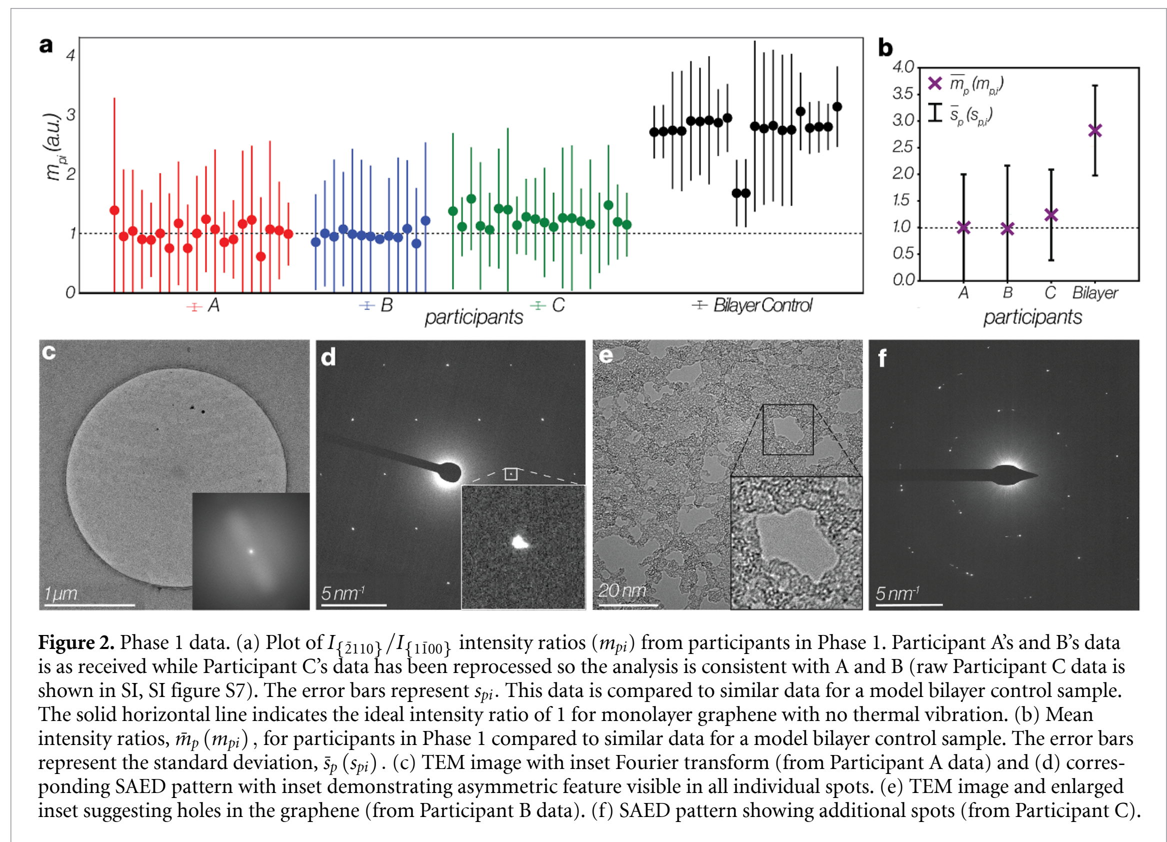

Figure 2. Phase 1 data. (a) Plot of $I_{\{\bar{2}110\}}/I_{\{1\bar{1}00\}}$ intensity ratios (m_{pi}) from participants in Phase 1. Participant A's and B's data is as received while Participant C's data has been reprocessed so the analysis is consistent with A and B (raw Participant C data is shown in SI, SI figure S7). The error bars represent s_{pi}. This data is compared to similar data for a model bilayer control sample. The solid horizontal line indicates the ideal intensity ratio of 1 for monolayer graphene with no thermal vibration. (b) Mean intensity ratios, $\bar{m}_p\,(m_{pi})$, for participants in Phase 1 compared to similar data for a model bilayer control sample. The error bars represent the standard deviation, $\bar{s}_p\,(s_{pi})$. (c) TEM image with inset Fourier transform (from Participant A data) and (d) corresponding SAED pattern with inset demonstrating asymmetric feature visible in all individual spots. (e) TEM image and enlarged inset suggesting holes in the graphene (from Participant B data). (f) SAED pattern showing additional spots (from Participant C).

as streaking of the diffraction peaks [48, 49]. Both sample tilt and streaking are known to change the measured diffraction intensities compared to flat suspended graphene [24, 50] so these factors can introduce larger variability in the diffraction spot intensities within a single pattern. Optical microscopy examination of all three TEM grids returned by the Phase 1 participants revealed visible damage to the graphene assigned to poor manual handling of the grids. It is therefore considered that this was likely to be a major cause of the large uncertainties.

To better assess whether the values of $m_{pi} > 1$ reported in Phase 1 indicate two or more layers of graphene, similar data was measured for a mechanically exfoliated 2LG sample as a control sample (figures 1(f) and 2(a), (b)). The thickness of the bilayer was independently verified by a combination of optical microscopy and AFM prior to transferring the flake onto the TEM chip. The majority of bilayer m_{pi} values are around 2.5, consistent with earlier experimental data reported for bilayer samples [29, 30]. However, two outlier values were found at around 1.7. Inspection of the raw SAED patterns for these outliers revealed that they had a large amount of amorphous contamination, generating a broad diffraction ring peaked close to the spatial frequency of graphene's first order diffraction peak (SI figure S9). In the absence of background subtraction, this will have the effect of increasing the intensity of the first order diffraction spots and supressing the value of the measured intensity ratio relative to the uncontaminated case, so these measurements were therefore removed from subsequent analysis of this bilayer control as erroneous values.

To compare different participants in Phase 1, we define $\bar{m}_p\left(m_{pi}\right)$ as the mean of all m_{pi} values where, p, refers to the participant and, i, to the SAED measurement (figure 2(b)). The variability within these values can be represented by the mean of the individual standard deviation, s_{pi}, values defined as $\bar{s}_p\left(s_{pi}\right)$. Comparing the aggregate data for Participants A–C in Phase 1 to the bilayer control reveals a significant difference for the CVD-grown graphene samples used in the study relative to the mechanically exfoliated bilayer. This gives confidence that the CVD-grown graphene samples analysed by participants are majority monolayer, consistent with expectations from optical microscopy prior to the transfer. However, the large error bars and limited data in Phase 1 means it is not possible to definitively determine whether the individual SAED with higher m_{pi} values are evidence of small bilayer regions.

2.1. Improvements to the measurement protocol after Phase 1

To address the different analysis methods used by participants in Phase 1 the measurement report spreadsheet for Phase 2 was changed to automatically calculate the mean intensity ratio (m_{pi}) and standard deviation (s_{pi}) from diffraction peak intensities for

each line scan. The SAED measurement protocol was also modified before releasing to the 16 international Phase 2 participants. Improvements are highlighted in SI section 2 and included emphasising care during manual handling. An accelerating voltage of 80 kV was also mandated for Phase 2. Although initial flexibility aimed to accommodate laboratories without 80 kV-aligned TEMs, one internal Phase 1 participant (Participant D) reported significant graphene damage at 200 kV, preventing their submission of SAED results. The minimum number of SAED patterns to be collected and analysed was also increased from 10 to 20 as the time required for this was not considered prohibitive. No modifications were made with respect to accurate TEM alignment as the scope of this study does not include specifying the alignment or calibration of a TEM system, and the ISO/TS 21356-2 standard already refers to other ISO standards outlining the basics of TEM operation.

3. Interlaboratory validation (Phase 2)

For Phase 2, 16 laboratories, including academia, national scientific institutes and industry, were sent a new CVD-grown graphene TEM grid and the revised measurement protocol. Participants 1–16 included representatives who regularly publish TEM measurements of 2D materials as well as those without experience of graphene characterisation. It also represented a broad geographical spread across the world, including Asia, Africa, Oceania, Europe and America. The calculated distributions of $m_{pi} \pm s_{pi}$ for Participants 1–15 are shown in figure 3(a) (total of 378 SAED and TEM image pairs). Participant 16's data initially appeared as an outlier with the highest accuracy and precision of all participants, ($m_{pi} = 0.99$ and $\bar{s}_p\left(s_{pi}\right) = 0.04$). However, closer inspection revealed their SAED data had a very high background signal and consequently a poor signal to background ratio (SBR) of 0.15 (where the SBR is calculated as $\frac{\text{signal}-\text{background}}{\text{noise}-\text{background}}$, see SI figure S10). This is likely due to incorrect detector calibration as the CCD camera should remove such a uniform background via the gain and dark references. Therefore, the data from Participant 16 was not included in the analysis, as it was determined to be erroneous. The measurement protocol did not have a background subtraction step so for a high background and low SBR, the m_{pi} intensity ratio will always be close to one. The data from Participants 1–15 has SBRs in the range 18–450, at least two orders of magnitude larger than Participant 16 (see SI figure S11) so the protocol was therefore revised to specify a minimum SBR of 10. Without removal, a non-zero background will reduce the measured intensity ratio in this data by up to 5.5%, calculated by adding a background matching the lowest experimental SBR to simulated data. Subtraction of background is therefore recognised to be beneficial for accurate SAED measurement. However, background subtraction was not made a requirement in the VAMAS protocol due to the challenge of prescribed fitting of the background in individual line profiles, because it is not usually done in published work and because it is not significant where the camera is properly calibrated and the graphene is clean. The signal to noise ratio was also measured from the experimental Phase 2 data and found to be in the range 18–2250, with the potential to change the measured intensity ratio by up to ±1.9%.

The mean value of all m_{pi} values for Participants 1–15 in Phase 2 is found to be 0.93 (middle and bold line in figures 3(a) and (b), respectively) with a root mean squared deviation (RMSD) of 0.20. Taking an uncertainty of the RMSD, values of $m_{pi} > 1.13$ are here considered to contain some bilayer contribution. This is consistent with our understanding from complementary analysis that the sample is predominantly monolayer. From other analyses (see SI figures S2–S4) we know that the sheets do contain some bilayer, and therefore some of the SAED data is likely from 2LG areas. In the further analysis we therefore exclude the clear outliers beyond twice the RMSD from the mean ($m_{pi} > 1.4$, and $m_{pi} < 0.5$). The upper limit excludes three of the 378 measurements (one from Participant 6 and two from Participant 10), meaning <1% of the sampled patterns are assigned to represent fully bilayer. This is consistent with Raman and AFM analysis although we note that ideally a similar SAED analysis of bilayer samples would be performed to more accurately assess variation in diffraction intensities for bilayer samples specifically, through a statistically relevant amount of data. The lower bound of $m_{pi} < 0.5$ excludes two SAED patterns (both Participant 4, which are believed to be the result of erroneous data, discussed subsequently). Yet, even when excluding these outliers, the Phase 2 data shows large differences in the mean intensity ratio values and standard deviations across participants (figures 3(a) and (b)), despite the improvements to the protocol introduced after Phase 1. We therefore seek to understand the factors that may contribute to this variability in order to develop improved recommendations for optimal acquisition, analysis and confidence in interpretation of SAED data for CVD-grown graphene films.

3.1. Contamination

Participant 4 reports an SAED pattern with the smallest measured intensity ratio, m_{pi}, value (0.33), as well as the largest mean uncertainty for their data set, $\bar{s}_p\left(s_{pi}\right) = 0.84$. Inspection of the accompanying TEM images shows the presence of particles on the graphene, with a diameter of 10–200 nm, in most of their data (see example in figure 3(c)). Subsequent STEM EDS analysis of the returned sample revealed

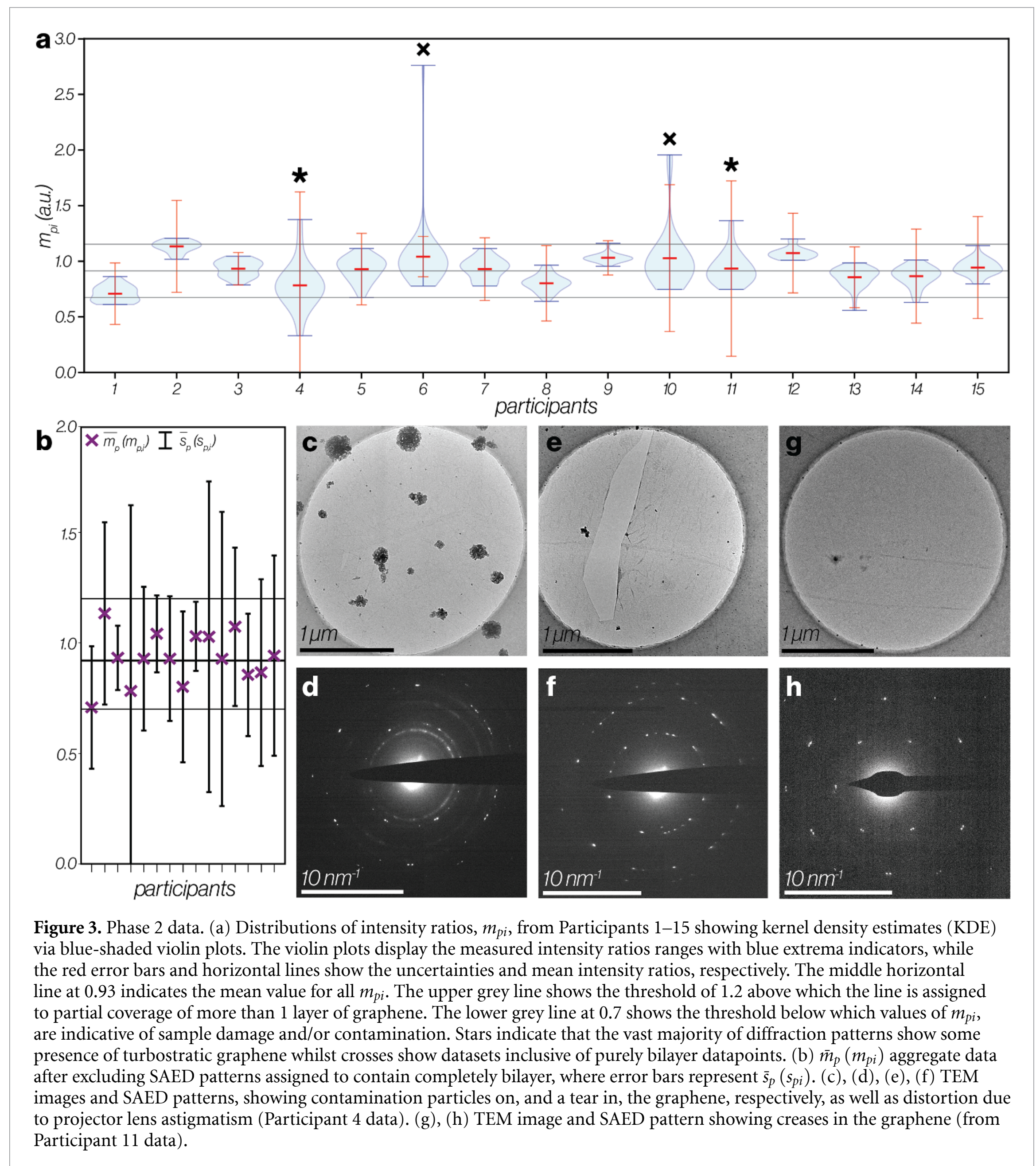

Figure 3. Phase 2 data. (a) Distributions of intensity ratios, m_{pi}, from Participants 1–15 showing kernel density estimates (KDE) via blue-shaded violin plots. The violin plots display the measured intensity ratios ranges with blue extrema indicators, while the red error bars and horizontal lines show the uncertainties and mean intensity ratios, respectively. The middle horizontal line at 0.93 indicates the mean value for all m_{pi}. The upper grey line shows the threshold of 1.2 above which the line is assigned to partial coverage of more than 1 layer of graphene. The lower grey line at 0.7 shows the threshold below which values of m_{pi}, are indicative of sample damage and/or contamination. Stars indicate that the vast majority of diffraction patterns show some presence of turbostratic graphene whilst crosses show datasets inclusive of purely bilayer datapoints. (b) $\bar{m}_p$ (m_{pi}) aggregate data after excluding SAED patterns assigned to contain completely bilayer, where error bars represent $\bar{s}_p$ (s_{pi}). (c), (d), (e), (f) TEM images and SAED patterns, showing contamination particles on, and a tear in, the graphene, respectively, as well as distortion due to projector lens astigmatism (Participant 4 data). (g), (h) TEM image and SAED pattern showing creases in the graphene (from Participant 11 data).

that these particles are composed of the elements Si, O, Au, Ca and Cl (SI figure S12). The presence of these nanoparticle contaminates produces a polycrystalline background with extra spots in the diffraction pattern, which can overlap with the graphene peaks. The very low value of intensity ratio obtained by Participant 4 is therefore likely due to these peaks contributing to increase the $I_{\{1\bar{1}00\}}$ peak intensities for the graphene. Such large contamination particles may also cause local deformation to the morphology of the graphene sheet, and it is recommended that such contaminated regions be avoided when seeking accurate thickness determination. Although the origin of this contamination is unknown, a potential source is hypothesised to be baking at too high a temperature or in a contaminated furnace. Other participants occasionally imaged similar particles but to a far lesser extent. Participant 4's data also showed tears in the carbon support film figure 3(e), similar to those that can be caused by surface tension from the drying of solvents or accidental exposure to moisture. Nonetheless, it is unclear what caused the contamination in this case.

3.2. Turbostratic graphene diffraction data

Some SAED patterns in Phase 2 also contained multiple sets of graphene diffraction spots with a rotational off-set between different sets (turbostratic graphene, as shown in figures 3(f) and (h)). Such additional lattice spots demonstrate that two different orientations of graphene coexist within the region sampled by the selected area aperture. This can occur

in 1LG due to a grain boundary, fold or tear. It can also occur in 2LG, where the second graphene layer is rotated in plane relative to the first (turbostratic 2LG) [51]. Inspection of the accompanying TEM images can often suggest whether tears or folds are likely to be responsible for the additional lattice spots (figures 3(f) and (h)), yet it is not possible to definitively distinguish if turbostratic graphene is responsible using the simple procedure outlined in the protocol provided to Phase 2 participants. The protocol was therefore modified after Phase 2, to include a further analysis step where more than one set of graphene spots are present in the SAED. In such cases, the sample is moved laterally by a distance corresponding to the radius of the selected area aperture on the sample while observing the SAED pattern. If the two sets of diffraction spots can be imaged separately the sample is then assumed to contain a grain boundary, tear, crease or fold. A representative SAED pattern should be recorded with only one set of diffraction spots and these are then analysed according to the normal procedure. On the other hand, if the two sets of diffraction spots cannot be separated by moving the sample, then the region is assumed to contain turbostratic graphene with a thickness of bilayer or greater and must be reported as such.

More than 40% of the m_{pi} measurements from Participants 4 and 11 contained turbostratic and/or defective regions within their SAED pattern and they also had the largest mean uncertainty ($\bar{s}_p >$ 0.75). The turbostratic patterns for Participant 4 are assigned to damage and contamination as already discussed but Participant 11 does not show similar issues. Instead, they are believed to have a high frequency of turbostratic patterns due to their use of a large selected area aperture (see SI figure S13). This is double the diameter of the aperture used by any other participant, meaning a larger sampling area and therefore more chance of measuring a second grain of CVD-grown graphene with a different crystal rotation. This larger sampling area will also result in a higher chance of detecting larger sample tilt or damage, which may be the origin of the larger standard deviations in Participant 11's data. The protocol was therefore modified after Phase 2 to require a selected area aperture size of less than 250 nm.

More accurate determination of the relative positions of the different crystals and their overlap for CVD-grown graphene can be obtained through centred dark field TEM imaging (see SI figure S14) [25], nano beam electron diffraction [16, 52, 53] or 4D-STEM [54] analysis. Analysis of the electron diffraction data from these techniques could be done in a similar way to that described in the SAED protocol, and all have the potential to improve the spatial resolution of the analysis from approximately hundreds of nanometres for SAED analysis to ∼1 nm for 4D-STEM. However, these techniques are more time consuming, more experimentally challenging and require more specialist TEM instrument alignment. Consequently, they are not included in the measurement protocol for the international standard which must take into account the cost for industry to undertake these standardised measurements and the availability of the measurement techniques. Here we confine our further analysis of the Phase 2 data to separating monolayer from more than one Bernal stacked graphene layers in single crystal SAED patterns. To do this we exclude the SAED patterns that contain more than one set of diffraction spots (highlighted by asterisks above the datasets in figure 3(a)). In addition, we exclude all data for participants where ⩾40% of the submitted SAED patterns contain diffraction spots from turbostratic graphene. The data from these participants (4 and 11) are considered erroneous due to the sample having been heavily damaged and the use of a large SAED aperture, respectively.

3.3. Electron fluence

Some of the TEM images from Phase 2 showed holes suggestive of electron beam induced damage to the graphene (SI figure S15). To assess the potential of electron beam damage reducing the accuracy of the measurement, we plot $\bar{s}_p$ for each participant in Phase 2 as a function of their reported electron fluence and flux (SI figure S16(a) and (b), respectively). Excluding the unusually large error of Participant 4 (the origin of which has already been discussed), this data shows a trend of increasing uncertainty at higher electron dose. The three participants with the lowest uncertainty in their reported measurements (Participants 3, 6 and 9) all report an electron flux of less than $\sim 10\ e^{-}Å^{-2}s^{-1}$ and therefore this value of maximum flux was added to the revised protocol. Although a lower electron flux will also reduce the intensity of the diffraction spots relative to the background, examination of the data from Participants 3, 6 and 9 show that SBRs of >10 are still readily achievable (see SI figure S11). The effect of varying flux, fluence, SBR and aperture size on the uncertainty is compared in SI figure S17. However, we recognise that there is significant interdependence in these factors, which makes separating their effects challenging.

3.4. Diffraction defocus and line profile positioning

Analysis errors are introduced in the diffraction peak intensity analysis where the line profile measurement is not precisely positioned over the maximum of the four diffraction peaks, which can be assumed to be in a straight line for an 80 keV electron beam. Most participants chose to use parallel illumination and a well-focussed (small) diffraction spot as this is commonly recommended for acquiring SAED diffraction data. However, small diffraction spots increase the challenge of ensuring that the intensity line profile accurately captures the highest intensity present in all the diffraction peaks it bisects.

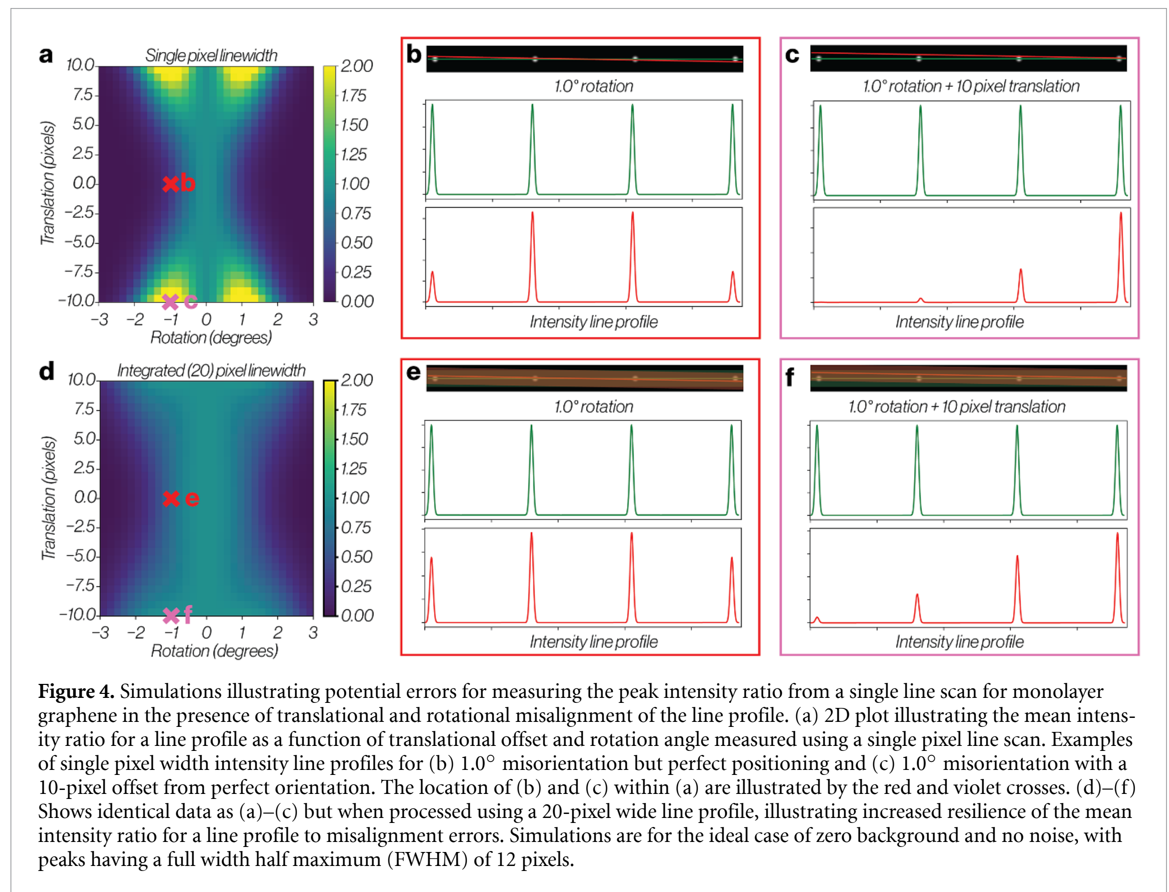

Figure 4. Simulations illustrating potential errors for measuring the peak intensity ratio from a single line scan for monolayer graphene in the presence of translational and rotational misalignment of the line profile. (a) 2D plot illustrating the mean intensity ratio for a line profile as a function of translational offset and rotation angle measured using a single pixel line scan. Examples of single pixel width intensity line profiles for (b) 1.0° misorientation but perfect positioning and (c) 1.0° misorientation with a 10-pixel offset from perfect orientation. The location of (b) and (c) within (a) are illustrated by the red and violet crosses. (d)–(f) Shows identical data as (a)–(c) but when processed using a 20-pixel wide line profile, illustrating increased resilience of the mean intensity ratio for a line profile to misalignment errors. Simulations are for the ideal case of zero background and no noise, with peaks having a full width half maximum (FWHM) of 12 pixels.

Figures 4(a)–(c) and supplementary video 1 show simulations to illustrate the large variation in measured intensity ratio that can arise due to inaccurate lateral or angular positioning of a single pixel line profile for perfect 1LG. When a single-pixel-width line profile is misaligned by an angular misalignment of 1° together with a 10-pixel translation (both possible within human error), a perfect 1LG SAED yields an erroneous value for $I_{\{\bar{2}110\}}/I_{\{1\bar{1}00\}}$ of 2.4, which would be assigned as bilayer. Increasing the line profile width to 20 pixels makes the analysis significantly more robust to positioning accuracy; retaining the $I_{\{\bar{2}110\}}/I_{\{1\bar{1}00\}}$ value of 1.0 for the same (1°, 10 pixels) misalignment (figures 4(d)–(f), supplementary video 2). Additionally, the presence of asymmetric distortion due to projector lens astigmatism, as seen in Participant 4's data (see figures 3(c)–(f)), will increase the likelihood of missing the diffraction peaks when positioning the line profile.

Increasing the width of the line profile also improves robustness of diffraction intensity measurements for Bernal stacked 2LG (SI figure S18) but can prevent diffraction patterns from turbostratic graphene being analysed where there is a small rotational misalignment. An alternative approach is acquiring the data with a slightly convergent beam or an under focused diffraction spot, as this broadens the individual diffraction peaks making it easier to correctly align the line profile. This approach is used by Participant 6 whose data shows under focused diffraction spots with the peak intensity spread over more than 25 pixels (see SI figure S19 for SAED pattern examples). Their measurements have one of the lowest deviations, with a $\bar{s}_p$ value of 0.17 (8.6%).

Inspection of all the participant data submitted in Phase 2 (see SI figure S20) showed that Participants 4, 10 and 11 used single pixel line profiles to analyse their SAED patterns and that they also had some of the largest individual uncertainties ($s_{pi} = 1.97$, 2.19 and 1.93 for Participants 4, 10 and 11, respectively). These participant's patterns were all reanalysed using line profile widths that exceeded the FWHM of the largest diffraction spot to ensure the maximum peak intensity was included in the line scan. However, although an improvement was observed (see SI figure S21), this had only a modest effect on the standard deviation, s_{pi}, likely due to the challenge of avoiding overlap with other diffraction peaks from contamination and turbostratic graphene. Nonetheless the protocol was revised to specify that line profiles must be extracted with a line profile width of greater than twice the FWHM of the largest diffraction spot. We note that the accuracy of the SAED analysis also depends on the type of camera used, through the camera's modulation transfer function, pixel resolution and area, as well as the TEM parameters used to acquire the diffraction data (camera length,

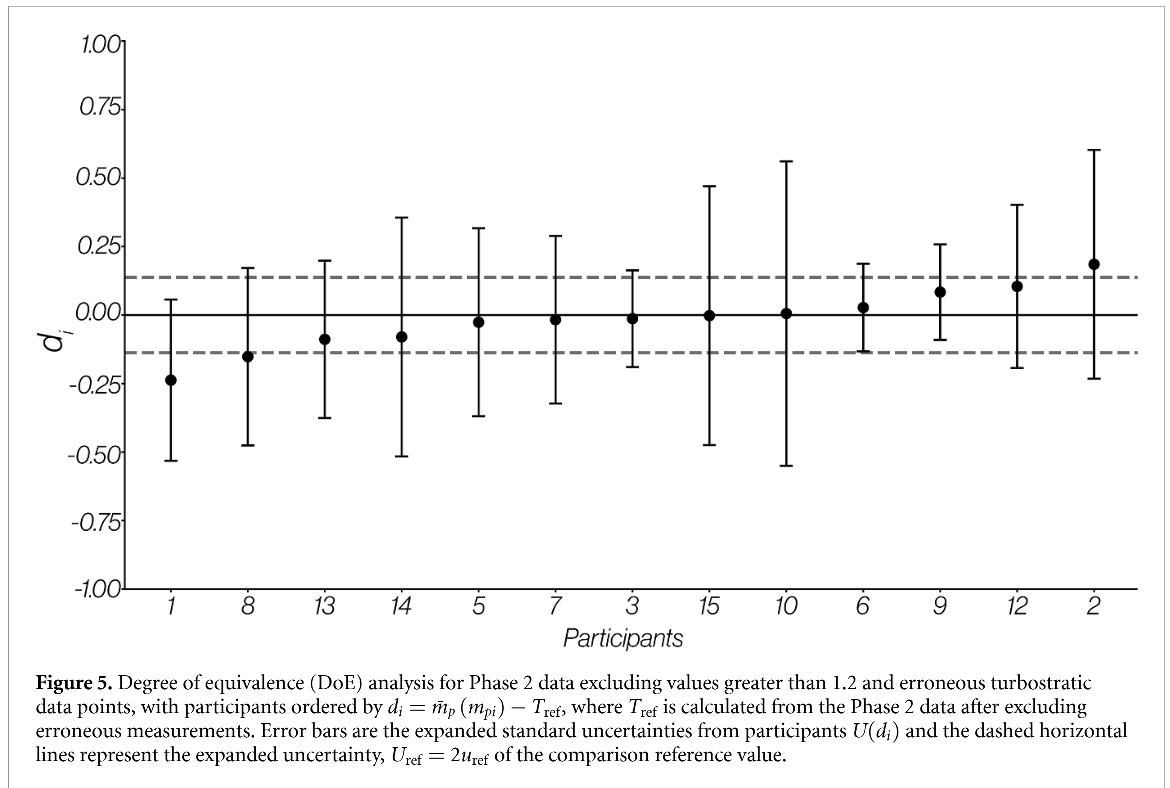

Figure 5. Degree of equivalence (DoE) analysis for Phase 2 data excluding values greater than 1.2 and erroneous turbostratic data points, with participants ordered by $d_i = \bar{m}_p(m_{pi}) - T_{\mathrm{ref}}$, where T_{ref} is calculated from the Phase 2 data after excluding erroneous measurements. Error bars are the expanded standard uncertainties from participants $U(d_i)$ and the dashed horizontal lines represent the expanded uncertainty, $U_{\mathrm{ref}} = 2u_{\mathrm{ref}}$ of the comparison reference value.

convergence angle, diffraction focus). However, these are highly interdependent and as there are a wide range of possible instrument configurations and suitable geometries, it is neither necessary nor practical to prescribe settings for these parameters in the protocol.

3.5. Degrees of equivalence analysis

To determine the accuracy and confidence in the comparability of measurement protocols tested through interlaboratory comparisons, particularly for international measurement standards, the 'degree of equivalence' (DoE) for the participants should be analysed. This illustrates the degree to which the values obtained following a standard measurement protocol are consistent with the reference value, expressed quantitatively as the deviation from the reference value and the uncertainty of this deviation [55]. The challenge for our analysis is that the reference value of the SAED intensity ratio for 1LG is unknown, due to the uncertainty in the effect of temperature on the scattered intensities through the Debye Waller factor. We therefore calculate a comparison reference value T_{ref} from uncertainty-weighted mean equations as part of the DoE analysis, as is typical for VAMAS studies [13, 56]. We perform this DoE analysis after removing partial bilayer data points with higher m_{pi} values ($m_{pi} > 1.2$ as a threshold value with a realistic precision that encompasses the variance observed in this study). We also removed the turbostratic SAED data points and erroneous data sets from Participants 4 and 11, where $\geqslant 40\%$ of their data was turbostratic. The resulting calculated DoE data for the as-received measurements in Phase 2 are shown in figure 5, with the participants ordered by their deviation from the reference value ($d_i = \bar{m}_p(m_{pi}) - T_{\mathrm{ref}}$). To calculate the uncertainty on this measurement, u_i, the mean uncertainty $\bar{s}_p$ (demonstrating the repeatability) and the sample homogeneity $s_{\mathrm{H}i}$ values for each participant are combined in quadrature. Analysis of $\bar{s}_p$ and $s_{\mathrm{H}i}$ values across all participants shows $\bar{s}_p$ dominates over $s_{\mathrm{H}i}$, (0.38 compared with 0.08). This reflects the expectation here that the inherent uncertainty of SAED data measurement, resulting from the many factors mentioned previously, is much larger than the inherent variability in the CVD 1LG. A comparison reference value T_{ref} is calculated from u_i and T_i, yielding a value of $T_{\mathrm{ref}} = 0.95$. The DoE expanded uncertainty, $U_i = 2u_i$ provides a confidence range of 95% [56], with $U_i = 0.14$. This DoE analysis suggests that CVD-grown graphene measured in this way can be assigned as monolayer for SAED data with a single set of graphene diffraction spots close to the [0001] zone axis where the intensity ratio of second to first order graphene diffraction peaks, $m_{pi} = 0.95 \pm 0.14$. Increased confidence regarding not excluding potential monolayer erroneously can be achieved with error bars of $3u_i$, yielding $m_{pi} = T_{\mathrm{ref}} \pm 3u_i = 0.95 \pm 0.21$.

Values of m_{pi} that are lower than this range suggest errors in the data, such as background due to contamination, sample damage and/or excessive fluence, all of which can cause an increase in the peak intensity for first order compared to the second

order diffraction peaks. Values of m_{pi} that are higher than this can be assigned to the presence of at least some fraction of two or more Bernal stacked graphene layers within the sampled SAED area, or significant translational and/or rotational misalignment of the line profile drawn when conducting analysis. Values of m_{pi} greater than $\sim$2 for non-erroneous data indicate full bilayer coverage. Figure 5 shows that the measurement protocol is robust and qualified, with no outliers. The DoE analysis can also assess the improvement when data previously analysed with single pixel intensity linewidths were reanalysed with integrated linewidths greater than twice the FWHM of a diffraction spot. We show this for a DoE analysis including all turbostratic data with Participants 4, 10 and 11 showing improvements to their DoE $u_i\,(d_i)$ of 0.4, 0.3 and 0.1 (24%, 19%, and 8%), respectively (see SI figure S21).

4. Conclusions

This large interlaboratory TEM study highlights the many sources of uncertainty associated with the use of SAED analysis for determining the presence of 1LG by TEM. The ratio of second: first order diffraction spot intensities in a SAED pattern is found to be a reliable means of determining the presence of 1LG but requires the sample be free from tears, strain and significant contamination. In the literature, a boundary condition of 1.0 is typically used as the limiting value for the intensity ratio of the second to first order diffraction spots ($I_{\{\bar{2}110\}}/I_{\{1\bar{1}00\}}<1.0$) when identifying 1LG. However, our results indicate that for practical measurements a higher threshold is appropriate. DoE analysis from our large data set of 294 SAED patterns shows that values of $I_{\{\bar{2}110\}}/I_{\{1\bar{1}00\}} = 0.95 \pm 0.14$ ($T_{\mathrm{ref}} \pm U_{\mathrm{ref}}$) are a reliable indicator of pristine 1LG. Yet within our combined data set from 15 international laboratories values of $I_{\{\bar{2}110\}}/I_{\{1\bar{1}00\}} = 0.93 \pm 0.20$ ($\bar{m} \pm$ RMSD) were still assigned to 1LG, with this larger variability assigned to measurement inaccuracies. To this end, we recommend a simple and realistic threshold value of $I_{\{\bar{2}110\}}/I_{\{1\bar{1}00\}} <1.2$ to assign 1LG, fully encompassing the relatively large uncertainties found through this study, even when following best practice. Values of $I_{\{\bar{2}110\}}/I_{\{1\bar{1}00\}} >1.2$ indicate the presence of at least partial bilayer material while values of $I_{\{\bar{2}110\}}/I_{\{1\bar{1}00\}} <0.7$ usually result from sample damage and/or amorphous surface contamination erroneously increasing the background for the first order graphene peaks. At an accelerating voltage of 80 kV, an electron flux of less than 10 $e^{-}\,\text{Å}^{-2}s^{-1}$ is recommended to minimise the chance of electron beam damage to the specimen, which can alter diffraction intensities. A small SAED aperture is preferred to reduce the chance of including multiple grains in the SAED pattern. Care should be taken when manually positioning the line profile on the SAED pattern, using a sufficiently large linewidth in the profile when recording the diffraction data. Overall, poor manual handling of the graphene was found to be the largest contributor to uncertainty in the ability to distinguish monolayer from 2LG using the SAED patterns.

Acknowledgments

This work was supported by the Engineering and Physical Sciences Research Council (EPSRC) for funding under Grants EP/X041204/1, EP/S021531/1, EP/Y024303/1, EP/M010619/1, EP/V001914/1 and EP/P009050/1, the National Physical Laboratory (NPL) UK (National Measurement System (NMS) of the Department for Science, Innovation and Technology (DSIT), UK, (Project #128807)) and the European Research Council (ERC) under the European Union's Horizon 2020 research and innovation programme (Grant ERC-2016-STGEvoluTEM-715502). TEM access at the University of Manchester was supported by the Henry Royce Institute for Advanced Materials, funded through EPSRC Grants EP/R00661X/1, EP/S019367/1, EP/P025021/1 and EP/P025498/1. We thank Diamond Light Source for access and support in use of the electron Physical Science Imaging Centre (instrument E02, Proposal Number MG29951) that contributed to the results presented here. Work at the Molecular Foundry was supported by the Office of Science, Office of Basic Energy Sciences, of the U.S. Department of Energy under Contract No. DE-AC02-05CH11231. Y.-C.Z thanks the funding support from the National Natural Science Foundation of China (Grant 12474026), and the Young Top Talents Program 2021QN02C068. SJH and ET thank Chris Livingston (NGI, University of Manchester) for his support and advice on the posting and receiving of TEM grids. RA acknowledges the support from the Spanish MICIU with funding from European Union Next Generation EU (PRTR-C17.I1) promoted by the Government of Aragon as well as from the Spanish MICIU (PID2023-151080NB-I00/AEI/10.13039/501100011033 and CEX2023-001286-S MICIU/AEI /10.13039/501100011033), the Government of Aragon (DGA) through the project E13 23R and the use of the facilities of the Laboratorio de Microscopias Avanzadas (LMA) at the Universidad de Zaragoza. AS and PLY thank the ARC Research Hub for Graphene Enabled Industry Transformation (IH150100003) and ARC Research Hub for Advanced Manufacturing with 2D Materials (IH210100025) for funding. AS and PLY also acknowledge the instruments and expertise of Microscopy Australia at Adelaide Microscopy, The University of Adelaide, enabled by NCRIS, university, and state government support.

Data availability statement

The data that support the findings of this study will be openly available following an embargo at the following URL/DOI: https://zenodo.org/uploads/15639586 [57].

Supplementary Information available at http://doi.org/10.1088/2053-1583/ae2ca1/data1.

Video 1- line profile alignment – thin line available at http://doi.org/10.1088/2053-1583/ae2ca1/data2.

Video 2- line profile alignment – thick line available at http://doi.org/10.1088/2053-1583/ae2ca1/data3.

Conflict of interest

The authors declare no competing interests.

Author contributions

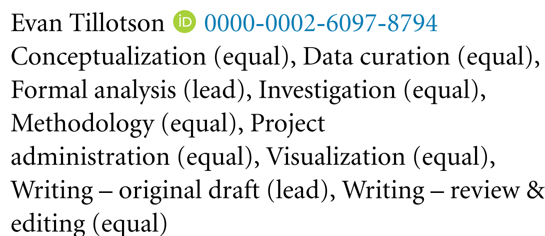
Evan Tillotson 0000-0002-6097-8794
Conceptualization (equal), Data curation (equal), Formal analysis (lead), Investigation (equal), Methodology (equal), Project administration (equal), Visualization (equal), Writing – original draft (lead), Writing – review & editing (equal)

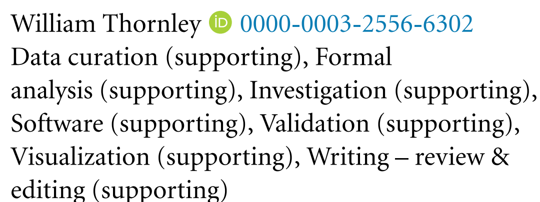
William Thornley 0000-0003-2556-6302
Data curation (supporting), Formal analysis (supporting), Investigation (supporting), Software (supporting), Validation (supporting), Visualization (supporting), Writing – review & editing (supporting)

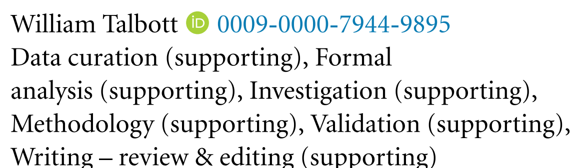
William Talbott 0009-0000-7944-9895
Data curation (supporting), Formal analysis (supporting), Investigation (supporting), Methodology (supporting), Validation (supporting), Writing – review & editing (supporting)

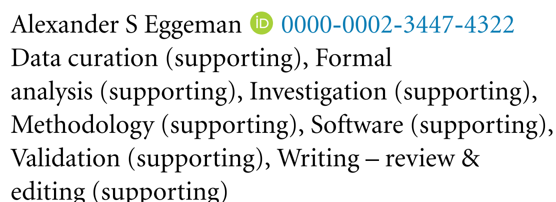
Alexander S Eggeman 0000-0002-3447-4322
Data curation (supporting), Formal analysis (supporting), Investigation (supporting), Methodology (supporting), Software (supporting), Validation (supporting), Writing – review & editing (supporting)

Daria Kriuchkova
Formal analysis (supporting), Investigation (supporting), Validation (supporting)

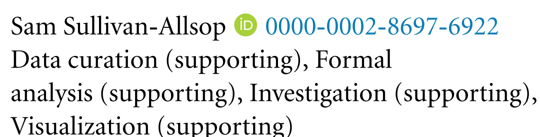
Sam Sullivan-Allsop 0000-0002-8697-6922
Data curation (supporting), Formal analysis (supporting), Investigation (supporting), Visualization (supporting)

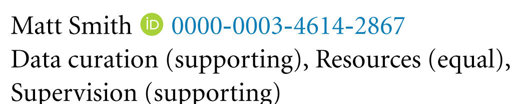
Matt Smith 0000-0003-4614-2867
Data curation (supporting), Resources (equal), Supervision (supporting)

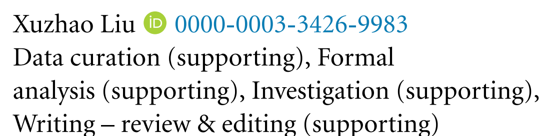
Xuzhao Liu 0000-0003-3426-9983
Data curation (supporting), Formal analysis (supporting), Investigation (supporting), Writing – review & editing (supporting)

Ashley Slattery 0000-0003-4023-3506
Data curation (supporting), Formal analysis (supporting)

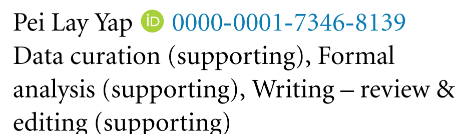
Pei Lay Yap 0000-0001-7346-8139
Data curation (supporting), Formal analysis (supporting), Writing – review & editing (supporting)

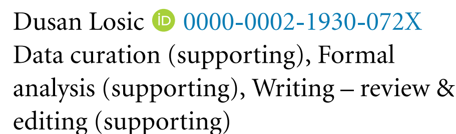
Dusan Losic 0000-0002-1930-072X
Data curation (supporting), Formal analysis (supporting), Writing – review & editing (supporting)

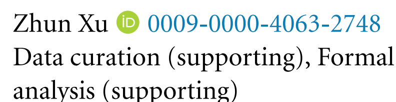
Zhun Xu 0009-0000-4063-2748
Data curation (supporting), Formal analysis (supporting)

Huan Wang
Data curation (supporting), Formal analysis (supporting), Writing – review & editing (supporting)

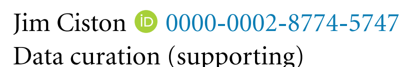
Jim Ciston 0000-0002-8774-5747
Data curation (supporting)

Alexander Rakowski
Data curation (supporting), Formal analysis (supporting)

Stephanie M Ribet 0000-0002-7117-066X
Data curation (supporting), Formal analysis (supporting)

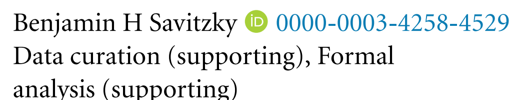
Benjamin H Savitzky 0000-0003-4258-4529
Data curation (supporting), Formal analysis (supporting)

Manfred E Schuster 0000-0003-3399-7372
Data curation (supporting), Formal analysis (supporting)

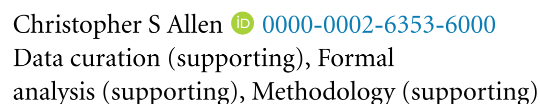
Christopher S Allen 0000-0002-6353-6000
Data curation (supporting), Formal analysis (supporting), Methodology (supporting)

Danielle Douglas-Henry
Formal analysis (supporting), Data curation (supporting)

Valeria Nicolosi 0000-0002-7637-4813
Data curation (supporting)

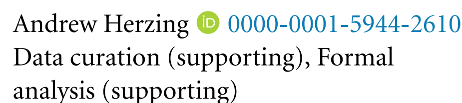
Andrew Herzing 0000-0001-5944-2610
Data curation (supporting), Formal analysis (supporting)

Jacques O'Connell 0000-0002-3758-3997
Data curation (supporting), Formal analysis (supporting)

Ezra J Olivier 0000-0002-4060-4023
Data curation (supporting), Formal analysis (supporting), Writing – review & editing (supporting)

Jan Neethling
Data curation (supporting), Formal analysis (supporting)

Yi-Chao Zou 0000-0002-4171-7185
Data curation (supporting), Formal analysis (supporting)

Ercin Duran 0000-0002-0674-3812
Data curation (supporting), Formal analysis (supporting), Investigation (supporting)

Rongsheng Cai
Data curation (supporting), Formal analysis (supporting)

Duc-The Ngo 0000-0001-6983-6058
Data curation (supporting), Formal analysis (supporting)

Roman Gorbachev 0000-0003-3604-5617
Data curation (supporting), Formal analysis (supporting), Writing – review & editing (supporting)

Jonas Haas
Data curation (supporting), Formal analysis (supporting)

Michael Schlegel 0009-0002-6809-0404
Data curation (supporting)

Jannik Meyer 0000-0003-4023-0778
Data curation (supporting), Formal analysis (supporting), Investigation (supporting), Writing – review & editing (equal)

Alba Centeno 0000-0001-8442-2283
Data curation (supporting), Writing – review & editing (supporting)

Amaia Pesquera
Data curation (supporting)

Amaia Zurutuza 0000-0001-6376-0224
Data curation (supporting)

Sungsu Kang 0000-0001-8220-0345
Data curation (supporting), Formal analysis (supporting)

Jungwon Park 0000-0003-2927-4331
Data curation (supporting), Formal analysis (supporting), Writing – review & editing (supporting)

Utkur Mirsaidov 0000-0001-8673-466X
Data curation (supporting), Formal analysis (supporting)

Colin Ophus 0000-0003-2348-8558
Data curation (supporting), Formal analysis (supporting)

Christian Rentenberger 0000-0002-3385-8850
Data curation (supporting), Formal analysis (supporting)

Thomas Waitz 0000-0002-9759-2983
Data curation (supporting), Formal analysis (supporting)

Jani Kotakoski 0000-0002-1301-5266
Data curation (supporting), Formal analysis (supporting)

Abhijit Roy
Data curation (supporting), Formal analysis (supporting)

Raul Arenal 0000-0002-2071-9093
Formal analysis (supporting), Funding acquisition (supporting), Methodology (equal), Writing – review & editing (supporting)

Andrew J Pollard 0000-0002-6841-2592
Conceptualization (equal), Data curation (equal), Formal analysis (equal), Funding acquisition (lead), Investigation (equal), Methodology (equal), Project administration (lead), Resources (equal), Supervision (equal), Validation (equal), Visualization (equal), Writing – original draft (equal), Writing – review & editing (equal)

Sarah J Haigh 0000-0001-5509-6706
Conceptualization (lead), Data curation (lead), Formal analysis (equal), Funding acquisition (lead), Investigation (equal), Methodology (equal), Project administration (equal), Resources (lead), Software (equal), Supervision (lead), Validation (equal), Visualization (equal), Writing – original draft (equal), Writing – review & editing (lead)

References

[1] Schedin F, Geim A and Novoselov K 2007 Detection of individual gas molecules adsorbed on graphene *Nat. Mater.* **6** 652–5

[2] Zhu Y *et al* 2011 Carbon-based supercapacitors *Science* vol 332 pp 1537–41

[3] Akinwande D, Petrone N and Hone J 2014 Two-dimensional flexible nanoelectronics *Nat. Commun.* **5** 1–12

[4] Cao Y, Fatemi V, Fang S, Watanabe K, Taniguchi T, Kaxiras E and Jarillo-Herrero P 2018 Unconventional superconductivity in magic-angle graphene superlattices *Nature* **556** 43–50

[5] Lee C, Wei X, Kysar J W and Hone J 2008 Measurement of the elastic properties and intrinsic strength of monolayer graphene *Science* **321** 385–8

[6] Castro Neto A H, Guinea F, Peres N M R R, Novoselov K S and Geim A K 2009 The electronic properties of graphene *Rev. Mod. Phys.* **81** 109–62

[7] Novoselov K S, Geim A K, Morozov S V and Jiang D 2004 Electric field effect in atomically thin carbon films *Phys. Rev. Lett.* **306** 666–9

[8] Ferrari A C *et al* 2006 Raman spectrum of graphene and graphene layers *Phys. Rev. Lett.* **97** 1–4

[9] Graf D, Molitor F, Ensslin K, Stampfer C, Jungen A, Hierold C and Wirtz L 2007 Spatially resolved raman spectroscopy of single- and few-layer graphene *Nano Lett.* **7** 238–42

[10] Dervishi E, Li Z, Shyaka J, Watanabe F, Biswas A, Umwungeri J L, Courte A, Biris A R, Kebdani O and Biris A S 2011 The role of hydrocarbon concentration on the synthesis of large area few to multi-layer graphene structures *Chem. Phys. Lett.* **501** 390–5

[11] Dervishi E, Li Z, Watanabe F, Biswas A, Xu Y, Biris A R, Saini V and Biris A S 2009 Large-scale graphene production by RF-cCVD method *Chem. Commun.* **30** 4061–3

[12] Hembacher S, Giessibl F J, Mannhart J and Quate C F 2003 Revealing the hidden atom in graphite by low-temperature atomic force microscopy *Proc. Natl Acad. Sci. USA* **100** 12539–42

[13] Bu T *et al* 2023 Thickness measurements of graphene oxide flakes using atomic force microscopy: results of an international interlaboratory comparison *Nanotechnology* **34** 225702

[14] Robertson A W, Bachmatiuk A, Wu Y A, Schäffel F, Rellinghaus B, Büchner B, Rümmeli M H and Warner J H 2011 Atomic structure of interconnected few-layer graphene domains *ACS Nano* **5** 6610–8

[15] Stone A J and Wales D J 1986 Theoretical studies of Icosahedral c60 and some related species *Chem. Phys. Lett.* **128** 501–3

[16] Meyer J C 2014 Transmission electron microscopy (TEM) of graphene *Graphene Prop. Prep. Characterisation Devices* (*Woodhead Publishing Series in Electronic and Optical Materials*)(Woodhead Publishing) pp 101–23

[17] Meyer J C *et al* 2011 Experimental analysis of charge redistribution due to chemical bonding by high-resolution transmission electron microscopy *Nat. Mater.* **10** 209–15

[18] Iakoubovskii K, Mitsuishi K, Nakayama Y and Furuya K 2008 Thickness measurements with electron energy loss spectroscopy *Microsc. Res. Tech.* **71** 626–31

[19] Egerton R F and Cheng S C 1987 Measurement of local thickness by electron energy-loss spectroscopy *Ultramicroscopy* **21** 231–44

[20] Carbone F, Kwon O H and Zewail A H 2009 Dynamics of chemical bonding mapped by energy-resolved 4D electron microscopy *Science* **325** 181–4

[21] Senga R, Lin Y-C, Morishita S, Kato R, Yamada T, Hasegawa M and Suenaga K 2022 Imaging of isotope diffusion using atomic-scale vibrational spectroscopy *Nature* **603** 68–72

[22] Steeds J W and Morniroli J-P 1992 Chapter 2: Selected Area Electron Diffraction (SAED) And Convergent Beam Electron Diffraction (CBED) *Minerals and Reactions at the Atomic Scale* (De Gruyte) pp 41

[23] Meyer J C, Geim A K, Katsnelson M I, Novoselov K S, Booth T J and Roth S 2007 The structure of suspended graphene sheets *Nature* **446** 60–63

[24] Meyer J C, Geim A K, Katsnelson M I, Novoselov K S, Obergfell D, Roth S, Girit C and Zettl A 2007 On the roughness of single- and bi-layer graphene membranes *Solid State Commun.* **143** 101–9

[25] Huang P Y *et al* 2011 Grains and grain boundaries in single-layer graphene atomic patchwork quilts *Nature* **469** 389–92

[26] Kazmierczak N P, Van Winkle M, Ophus C, Bustillo K C, Carr S, Brown H G, Ciston J, Taniguchi T, Watanabe K and Bediako D K 2021 Strain fields in twisted bilayer graphene *Nat. Mater.* **20** 956–63

[27] Meyer J C 2021 Transmission Electron Microscopy Characterization Of Graphene *Graphene: Properties, Preparation, Characterization and Applications* 2nd edn (Elsevier) (https://doi.org/10.1016/B978-0-08-102848-3.00013-X)

[28] Wang M *et al* 2021 Single-crystal, large-area, fold-free monolayer graphene *Nature* **596** 519–24

[29] Su Y 2022 Characterizations of Carbon Nanotubes and Graphene *High-Performance Carbon-Based Optoelectronic Nanodevices* 1st edn vol 319 (Springer)

[30] Hernandez Y *et al* 2008 High-yield production of graphene by liquid-phase exfoliation of graphite *Nat. Nanotechnol.* **3** 563–8

[31] Horiuchi S *et al* 2003 Carbon nanofilm with a new structure and property *Jpn. J. Appl. Phys.* **42** L1073

[32] Wang S *et al* 2023 Controlled growth of bilayer graphene on space-confined Cu substrates *J. Phys. Chem. C* **127** 13601–8

[33] Kumar S, McEvoy N, Lutz T, Keeley G P, Nicolosi V, Murray C P, Blau W J and Duesberg G S 2010 Gas phase controlled deposition of high quality large-area graphene films *Chem. Commun.* **46** 1422–4

[34] Lu C-C, Lin Y-C, Liu Z, Yeh C-H, Suenaga K and Chiu P-W 2013 Twisting bilayer graphene superlattices *ACS Nano* **7** 2587–94

[35] Susi T, Madsen J, Ludacka U, Mortensen J J, Pennycook T J, Lee Z, Kotakoski J, Kaiser U and Meyer J C 2019 Efficient first principles simulation of electron scattering factors for transmission electron microscopy *Ultramicroscopy* **197** 16–22

[36] Zhang X, Sun L, Guo X, Wang P, Yu F, Dong Z and Pan E 2025 Single-layer graphene film-based microacoustic pressure sensing through confinement-enhanced reaction engineering *ACS Appl. Nano Mater.* **8** 19055–64

[37] Sung S H *et al* 2019 Stacking, strain, and twist in 2D materials quantified by 3D electron diffraction *Phys. Rev. Mater.* **3** 1–9

[38] Sun L, Howell S E L, Brady M, Xu X and McNeil K 2021 Hetero-site nucleation for growing twisted bilayer graphene with a wide range of twist angles *Nat. Commun.* **12** 2391

[39] Wilson N R *et al* 2009 Graphene oxide: structural analysis and application as a highly transparent support for electron microscopy *ACS Nano* **3** 2547–56

[40] Ren H, Xia X, Sun Y, Zhai Y, Zhang Z, Wu J, Li J and Liu M 2024 Electrolyte engineering for the mass exfoliation of graphene oxide across wide oxidation degrees *J. Mater. Chem. A* **12** 23416–24

[41] Tewary V K and Yang B 2009 Singular behavior of the Debye-Waller factor of graphene *Phys. Rev. B* **79** 1–5

[42] Butz B, Dolle C, Niekiel F, Weber K, Waldmann D, Weber H B, Meyer B and Spiecker E 2014 Dislocations in bilayer graphene *Nature* **505** 533–7

[43] Pacilé D, Meyer J C, Fraile Rodríguez A, Papagno M, Gómez-Navarro C, Sundaram R S, Burghard M, Kern K, Carbone C and Kaiser U 2011 Electronic properties and atomic structure of graphene oxide membranes *Carbon* **49** 966–72

[44] Cancado L G, Jorio A, Ferreira E H M, Stavale F, Achete C A, Capaz R B, Moutinho M V O, Lombardo A, Kulmala T S and Ferrari A C 2011 Quantifying defects in graphene via Raman spectroscopy at different excitation energies *Nano Lett.* **11** 3190–6

[45] Pollard A J *et al* 2017 Good practice guide (145) characterisation of the structure of graphene *Natl Phys. Lab.* **2** 90–101 (available at: https://www.npl.co.uk/resources/gpgs/graphene-structure-characterisation)

[46] Kirkland E J 2010 *Advanced Computing in Electron Microscopy* 3rd edn (Springer) p 354

[47] Eggeman A S, London A and Midgley P A 2013 Ultrafast electron diffraction pattern simulations using GPU technology. Applications to lattice vibrations *Ultramicroscopy* **134** 44–47

[48] Mao Y, Wang W L, Wei D, Kaxiras E and Sodroski J G 2011 Graphene structures at an extreme degree of buckling *ACS Nano* **5** 1395–400

[49] Nelson R and Peliti L 1987 Fluctuations in membranes with and hexatic order *J. Phys.* **48** 1085–92

[50] Robertson A W, Bachmatiuk A, Wu Y A, Schäffel F, Büchner B, Rümmeli M H and Warner J H 2011 Structural distortions in few-layer graphene creases *ACS Nano* **5** 9984–91

[51] Matassa R, Orlanducci S, Tamburri E, Guglielmotti V, Sordi D, Terranova M L, Passeri D and Rossi M 2014 Characterization of carbon structures produced by graphene self-assembly *J. Appl. Crystallogr.* **47** 222–7

[52] Caplins B W, Holm J D and Keller R R 2019 Orientation mapping of graphene in a scanning electron microscope *Carbon* **149** 400–6

[53] Kim K, Lee Z, Regan W, Kisielowski C, Crommie M F and Zettl A 2011 Grain boundary mapping in polycrystalline graphene *ACS Nano* **5** 2142–6

[54] Caplins B W, Holm J D, White R M and Keller R R 2020 Orientation mapping of graphene using 4D STEM-in-SEM *Ultramicroscopy* **219** 113137

[55] Kacker R N, Datla R U and Parr A C 2003 Statistical interpretation of key comparison reference value and degrees of equivalence *J. Res. Natl Inst. Stand. Technol.* **108** 439–46

[56] (ISO 13528:2022) 2022 INTERNATIONAL STANDARD in proficiency testing (International Organisation for Standardization) Statistical methods for use in proficiency testing by interlaboratory comparison (https://doi.org/10.3403/30237515)

[57] Tillotson E 2026 VAMAS Interlaboratory Graphene SAED data *Zenodo* (available at: https://zenodo.org/records/15639586)